

## 6 | Evolution of star clusters in an evolving spiral galaxy

*Based on:*

*Steven Rieder, Robert Crain, Tom Theuns, Joop Schaye and Simon Portegies Zwart  
Evolution of star clusters in an evolving spiral galaxy  
In preparation*

In this chapter, we simulate open star clusters in a live galaxy. We utilize the tidal tensor approach described in chapter 5 to study the evolution and survivability of open clusters for various tidal fields representative for galactic open clusters. In the calculations, we include the effects of an initial cluster mass and radius distribution, a stellar initial mass function and stellar evolution, while the simulated galaxy has a potential representative for the Milky Way.

We simulate a set of 100 clusters in each of 30 different tidal fields, and compare the surviving distribution of clusters to the observed distribution of open clusters in the Milky Way.

## 6.1 Introduction

The stellar population of the galactic disk in the Milky Way is mostly comprised of field stars, while some stars reside in open clusters. However, most of these field stars were at one point not isolated: they used to be part of a cluster or a more extended association of stars (Portegies Zwart et al. 2010b; Lada and Lada 2003). Only a few stars remain bound to their birth cluster for more than a Gyr, most open clusters are disrupted within a few 100 Myr (e.g. Oort 1958; Kharchenko et al. 2005)

The mechanisms responsible for dispersing clusters and associations include stellar evolution, spiral arms, giant molecular clouds and a general galactic tidal field. Lamers and Gieles (2006) modelled the dissolution of open clusters, combining the effects of stellar evolution, tidal stripping, spiral arm shocks and GMC encounters using disruption rates found for these different disruption mechanisms in earlier studies, assuming a circular orbit around the galaxy at solar radius. They found a good agreement for cluster lifetimes between their cluster sample and observed clusters, with disruption of the clusters largely due to encounters with Giant Molecular Clouds (GMCs).

In this chapter, we use self-consistent simulations of star clusters in an evolving Milky Way-like galaxy to determine the lifetime and evolution of open clusters. We make use of a Milky Way-like galaxy re-simulation (originally selected from the large-scale Millennium run Springel et al. (2005)), which includes dark matter, gas and stars. The star particles in this simulation represent down to  $10^5 M_{\odot}$  in stellar matter, and contain information about their formation time, metallicity and location in each snapshot. We use these particles to trace the orbits of star clusters that would be born at such locations, giving us a realistic representation of the orbits star clusters would have in a Milky Way-type galaxy.

We calculate the tidal field in each snapshot at the location of these star particles, giving us a time-dependent tidal field for individual star clusters. With the Astrophysical Multipurpose Software Environment (AMUSE, Portegies Zwart et al. 2013), we combine these tidal fields to simulations of individual star clusters (including a stellar initial mass function and stellar evolution), giving us a self-consistent model for star clusters in the Milky Way.

We investigate the mass and radius distribution of clusters as they evolve, and compare the mass and radius distribution of surviving clusters to observations of open clusters in the solar neighbourhood. We distinguish clusters based on tidal field strength and orbital eccentricity, and investigate a possible signature of the tidal field strength in observable properties of the clusters.

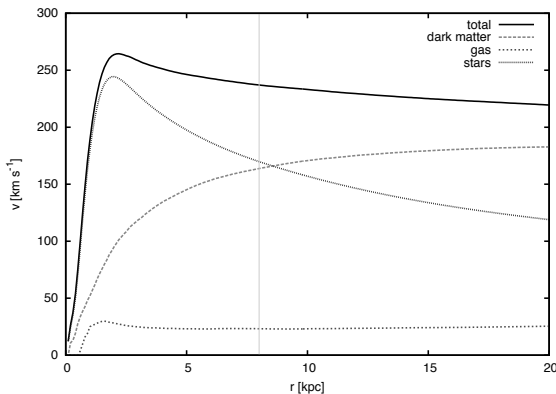


**Figure 6.1:** The rotation curve of the simulated galaxy employed in this chapter. The vertical line indicates the velocities at 8 kpc, the radius at which we select the star particles.

## 6.2 The experimental setup

### 6.2.1 The galaxy simulation

As a large-scale environment, we take a galaxy selected from re-simulated galaxies from the Millennium run (Springel et al. 2005). We selected this galaxy as a good example for a Milky Way-like galaxy, in that it has no major encounters after  $z = 1$  and has a stellar disk similar to that of the Milky Way. In Figure 6.1 we plot the galaxy's rotation curve, and in Figure 6.2 shows the distribution of gas in our simulated galaxy at  $z = 0$ .

The code used for the re-simulation is an evolution of the GIMIC and OWLS code, which reproduces many observable aspects of Milky Way-like galaxies at low redshift (eg Crain et al. 2009; Haas et al. 2012, and references therein). The simulation starts with only dark matter and gas particles. When a gas particle reaches a temperature and density required for star formation, it is converted to a star particle, with metallicity fixed at this point. Stellar winds, supernovae and other types of feedback incorporated in terms of subgrid physics gradually cause these star particles to lose mass to their surrounding gas particles, which are then enriched with metals formed in the stars.

We take a total of 900 snapshots during the galaxy simulation, with 23 Myr between snapshots near  $z = 0$ . This is sufficient time to account for orbits at the Solar orbital radius, with approximately 10 snapshots for each circular orbit between which we can interpolate. In each snapshot, the masses, positions and velocities of all the star, gas and dark matter particles are saved, as well as the metallicity, time of formation (when a gas particle is converted to a star particle), and mass at time of formation for the star particles.

From the final snapshot, we select all star particles and use these to calculate

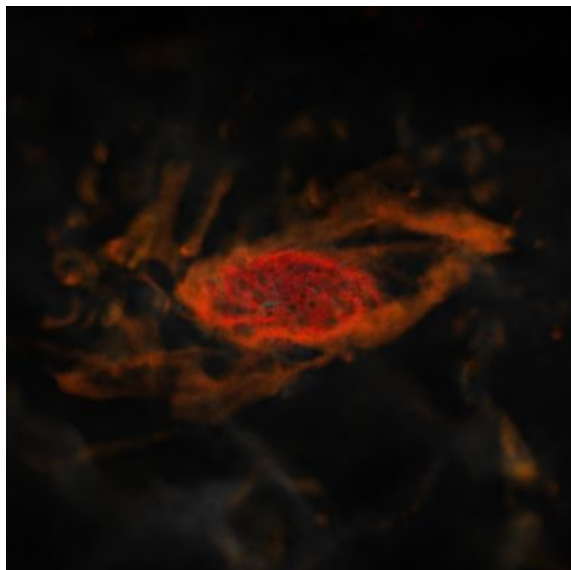


**Figure 6.2:** Image of gas in the galaxy used in our simulation at  $z = 0$ . Brightness and colour correspond to gas density and temperature, respectively.

the centre of the galaxy by taking the median of the positions. We calculate the orientation of the galactic stellar disk using the moment of inertia tensor. We then transform the positions of the star particles to galactic coordinates, and select all star particles with  $r = 8 \pm 0.5$  kpc and  $z = 0 \pm 0.5$  kpc. For each of these particles, we calculate the tidal tensor using the method described in Renaud et al. (2011) and chapter 5 with the gravity code Fi (Pelupessy 2005).

We now have fully time-dependent tidal fields for each of these star particles. These are representative for the tidal fields experienced by open clusters, but not for the stars expelled from these clusters. The initial mass of the star particles generally varies between  $2 \times 10^5 M_{\odot}$  and  $4 \times 10^5 M_{\odot}$ . This is higher than the mass of most open clusters, indicating that we cannot use their mass as a cluster mass function.

## 6.2.2 Star cluster models

We generate a set of initial conditions for cluster simulations. For these clusters, we use a Plummer (1911) model to spatially distribute stars. For the initial mass function of the stars, we select a Kroupa (2001) IMF, with a lower-mass cut-off at  $0.1 M_{\odot}$ . The average stellar mass varies between  $0.33$  and  $0.38 M_{\odot}$ , this scatter is due to run-to-run variations.

For the star clusters, we draw their initial masses from a Schechter (1976) distribution:

$$NdM \propto M^{-2} \exp(-M/M_{\star})dM, \quad (6.1)$$

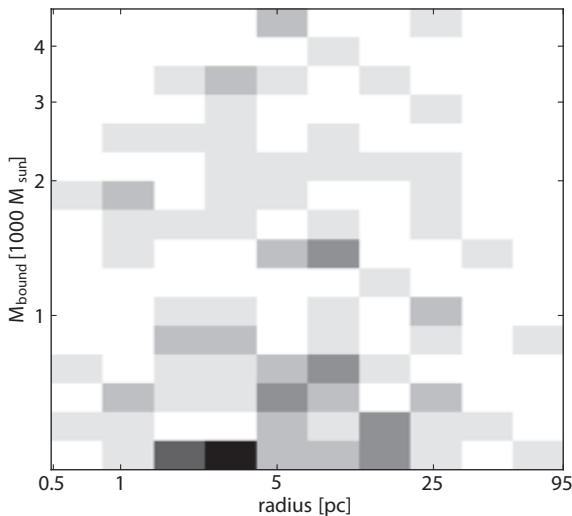


**Figure 6.3:** Density distribution of 100 randomly sampled clusters from a Schechter mass distribution and a lognormal radius distribution.

where  $M_* = 2 \times 10^5 M_\odot$ , which Larsen (2009) determined to be a good fit for young star clusters in spiral galaxies. For this initial investigation, we constrain our sample to those masses between  $5 \times 10^2 M_\odot$  and  $5 \times 10^3 M_\odot$ : lower mass clusters will quickly disperse, while higher mass clusters would take a much longer time to calculate. The minimum total mass for star clusters in our sample is  $500 M_\odot$ , the maximum is set to  $5000 M_\odot$ .

For the radius, we use a LogNormal distribution, with a mean of 5 pc and  $\sigma = 3$  pc. This is shown to be a good fit for young open clusters (van den Heuvel and Portegies Zwart 2013). We sample a total of 100 clusters from this distribution. This sample is limited to radii between 0.4 pc and 100 pc, again due to computational constraints. In Figure 6.3 we show the density distribution of clusters sampled this way.

### 6.2.3 Embedding star clusters in the galaxy

We use the AMUSE (Portegies Zwart et al. 2013) framework to simulate these clusters with the selected tidal fields. In AMUSE, many different codes for simulating gravity and stellar evolution are available. In order to investigate a large number of different clusters, we use the fast GPU-enabled tree code Bonsai (Bédorf et al. 2012) for gravity, in combination with the SeBa code (Portegies Zwart and Verbunt 1996; Toonen et al. 2012) for stellar evolution. We previously (see Figure 5.7) determined that the Bonsai code is indeed suitable for star cluster calculations, despite being a tree code. We use the mechanism described in chapter 5 to simulate the clusters within a time-dependent tidal field.

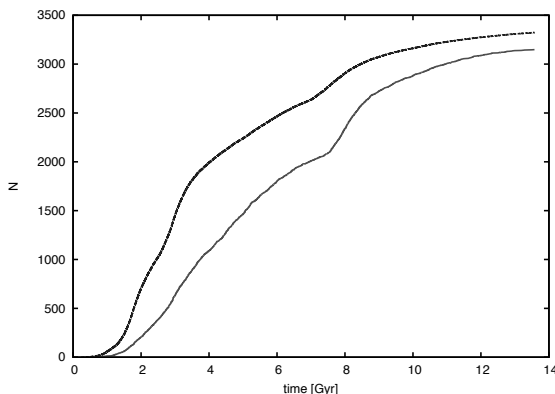


**Figure 6.4:** Star formation times for each of the star particles selected in our sample (solid) and for all the stars in our galaxy, lowered by 2 dex (dashed).

From our region of interest in the galaxy, we obtained 3150 star particles. In Figure 6.4, we plot the formation time for these particles. Since observed clusters only live for up to one Gyr, we select those particles that formed within a slightly longer period than that, up to 1.2 Gyr, to investigate in this chapter. For each of these star particles, we calculate the time-dependent tidal tensor, and simulate the previously generated set of 100 star clusters with this tensor.

At each step in the simulation, we check if the cluster still survives, i.e. more than 10% of the initial number of stars is still bound to the cluster. We stop the simulation at  $z = 0$ , or if the cluster is disrupted. If the cluster survives until  $z = 0$ , we save the positions, velocities and other properties of the stars in order to investigate these further.

## 6.3 Results

### 6.3.1 Tidal fields

We investigate all tidal fields formed in the last 1.5 Gyr of the simulation. In these fields, we distinguish three components: the dark matter, stars and gas. In Figure 6.5, we display two representatives of these tidal fields.

The tidal field is dominated by the stellar component, while the role of dark matter is almost equally important. The gas component is significantly less pronounced. This behaviour is as expected from the relative contributions of each fraction to the total enclosed mass, as can be inferred from Figure 6.1.

We find that the strength of the tidal field - measured as the largest component of its eigenvalues  $\lambda_{\max}$  - varies between  $0.0006 \text{ Myr}^{-2}$  and  $0.0084 \text{ Myr}^{-2}$ . Variations over time in the individual tidal fields are clearly visible, and are due to various causes, such as the eccentricity of the orbit, passages through the stellar

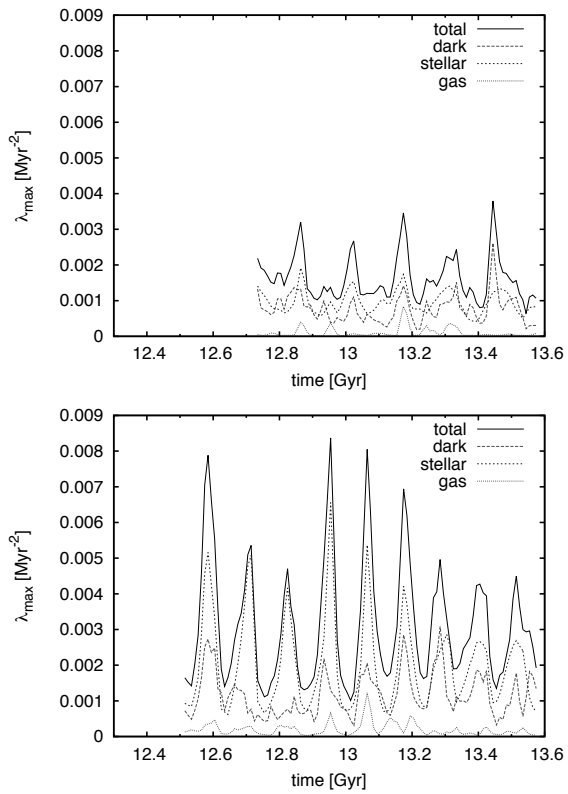


**Figure 6.5:** Strength ( $\lambda_{\max}$ ) of two tidal fields, 24 (top) as a representative weak tidal field and 33 (bottom) as a representative strong tidal field. The contributions of the three components (dark matter, stars and gas) are indicated.

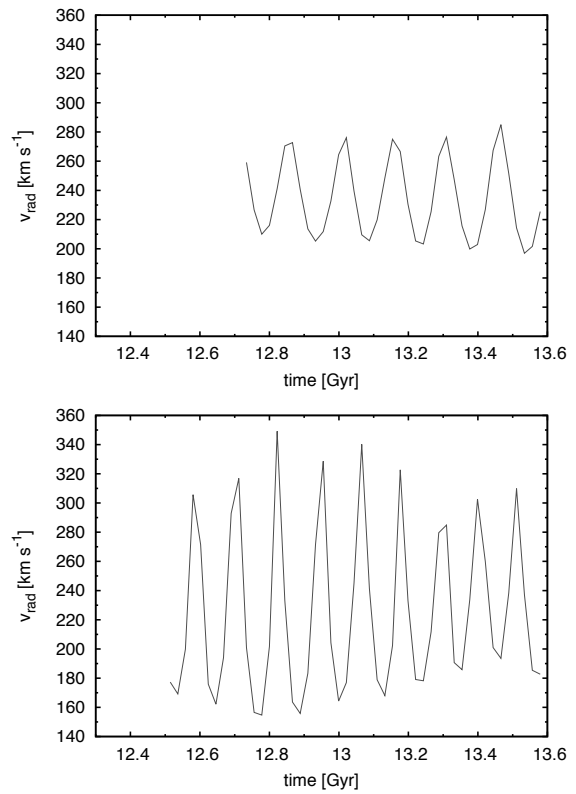


**Figure 6.6:** Orbital (circular) velocities of two clusters, 24 (top) and 33 (bottom).



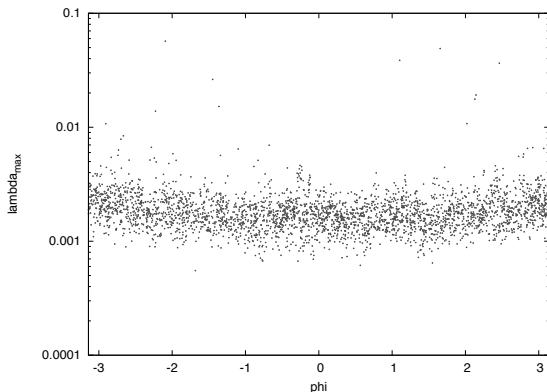


**Figure 6.7:** Distribution of tidal field strengths for clusters with different orbital phases at  $z = 0$ .

disk and encounters with locally enhanced densities. While in most tidal fields the difference between peaks and valleys is about a factor 2-3, in some extreme cases the difference can be a factor 9. In such cases (such as tidal field 30, see Table 6.1), a strong correlation is visible between the tidal field strength and the radial velocity of the cluster (see Figure 6.6), e.g. the eccentricity of the orbit.

The orbital periods of the clusters is most clearly visible in the stellar component, which shows one peak per orbit around the galactic centre. In the gas and dark matter components, this periodicity is far less pronounced.

For each of the clusters, we calculate the instantaneous Kepler orbital parameters: the eccentricity and the semi-major axis of the orbit. We find that the clusters with the strongest variations in the tidal field are those on the most eccentric orbits. In Table 6.1 we show the orbital parameters and tidal field strengths for each of the tidal fields studied in this chapter.

In Figure 6.7, we plot the field strength  $\lambda_{\max}$  against the orbital phase  $\phi$  in the final snapshot. We find that the tidal fields have a mean value of  $0.00196 \text{ Myr}^{-2}$  with a standard deviation  $\sigma = 0.00187 \text{ Myr}^{-2}$ .

### 6.3.2 Cluster evolution

We simulate clusters with each of the tidal fields investigated in the previous section. For each of the clusters simulated this way, we track the half-mass radii and the bound masses over their lifetimes.

We find that all clusters with a lifetime  $> 1.1 \text{ Gyr}$  are destroyed at  $z = 0$ . The rate at which clusters lose mass varies, dependent on the strength of the individual tidal fields and their initial compactness. Clusters that are initially more extended than  $10 \text{ pc}$  are destroyed within  $100 \text{ Myr}$ . The influence of peaks in the tidal field is visible, although these variations are largely smoothed out over a cluster's lifetime.

**Table 6.1:** Properties for the individual tidal fields investigated in this chapter.

ID	$Z$	$t_{\text{start}}$ Myr	$r(z=0)$ kpc	$e$	$a$ kpc	$p$ Myr	$\lambda_{\text{max}}(\text{min})$ $\text{Myr}^{-2}$	$\lambda_{\text{max}}(\text{max})$ $\text{Myr}^{-2}$	$\langle \lambda_{\text{max}} \rangle$ $\text{Myr}^{-2}$
02	0.022	13526.3	7.707	0.116	6.971	171.3	0.00230	0.00270	0.00244
03	0.014	13489.7	7.642	0.770	5.800	130.4	0.00148	0.00785	0.00436
04	0.020	13344.6	8.139	0.065	8.704	233.5	0.00066	0.00284	0.00136
05	0.035	13276.2	7.868	0.035	7.976	207.8	0.00107	0.00292	0.00201
06	0.026	13267.8	7.783	0.114	8.724	238.8	0.00098	0.00335	0.00183
07	0.045	13244.2	8.379	0.071	8.482	221.9	0.00124	0.00278	0.00189
08	0.048	13205.5	8.376	0.288	6.506	149.1	0.00100	0.00431	0.00237
09	0.024	13182.9	7.526	0.156	8.419	229.6	0.00183	0.00358	0.00269
10	0.017	13101.6	8.384	0.128	7.507	184.7	0.00103	0.00372	0.00202
11	0.029	12994.0	7.601	0.167	6.767	164.8	0.00137	0.00352	0.00242
12	0.008	12952.9	7.997	0.037	8.096	211.1	0.00074	0.00485	0.00218
13	0.015	12929.0	7.939	0.299	7.257	179.7	0.00144	0.00463	0.00298
14	0.045	12922.2	7.841	0.062	7.910	205.6	0.00141	0.00375	0.00243
15	0.022	12915.9	8.437	0.281	7.317	177.3	0.00059	0.00372	0.00155
16	0.006	12884.6	8.007	0.108	8.889	242.7	0.00075	0.00311	0.00164
17	0.022	12847.4	8.307	0.064	7.945	201.9	0.00113	0.00307	0.00206
18	0.046	12837.7	8.384	0.238	8.879	237.6	0.00071	0.00276	0.00157
19	0.023	12768.0	8.180	0.150	7.207	175.6	0.00106	0.00347	0.00192
20	0.018	12762.7	7.982	0.129	7.692	195.6	0.00142	0.00357	0.00221
21	0.023	12746.7	7.643	0.131	8.296	223.1	0.00108	0.00471	0.00204
22	0.026	12736.1	8.003	0.162	9.515	268.8	0.00079	0.00315	0.00142
23	0.037	12720.1	8.463	0.113	8.481	221.0	0.00079	0.00394	0.00186
24	0.004	12719.6	8.282	0.125	8.139	209.7	0.00064	0.00379	0.00163
25	0.049	12719.6	7.670	0.034	7.896	206.9	0.00174	0.00414	0.00281
26	0.028	12707.1	7.672	0.309	5.876	132.8	0.00165	0.00520	0.00330
27	0.050	12695.5	8.018	0.144	7.639	193.2	0.00120	0.00349	0.00202
28	0.027	12610.2	8.362	0.178	10.167	291.5	0.00120	0.00303	0.00182
29	0.036	12578.9	7.591	0.220	9.730	284.2	0.00130	0.00451	0.00241
30	0.022	12563.1	8.357	0.223	6.937	164.3	0.00076	0.00271	0.00164
31	0.030	12563.1	7.688	0.025	7.501	191.4	0.00137	0.00454	0.00273
32	0.035	12523.2	8.320	0.088	8.437	220.8	0.00103	0.00345	0.00203
33	0.026	12509.3	8.311	0.393	5.995	132.3	0.00101	0.00837	0.00314
34	0.024	12506.0	7.600	0.062	7.696	199.8	0.00093	0.00330	0.00199
35	0.010	12434.1	8.086	0.585	5.453	116.1	0.00081	0.00721	0.00331
36	0.010	12334.3	7.816	0.049	8.102	213.4	0.00100	0.00438	0.00236
37	0.028	12324.1	8.247	0.584	5.866	128.5	0.00065	0.00840	0.00296
38	0.053	12323.8	7.640	0.122	8.552	233.6	0.00087	0.00318	0.00178
39	0.029	12313.8	7.722	0.139	8.900	246.9	0.00081	0.00443	0.00189
40	0.006	12303.4	7.580	0.126	6.754	164.5	0.00108	0.00340	0.00220

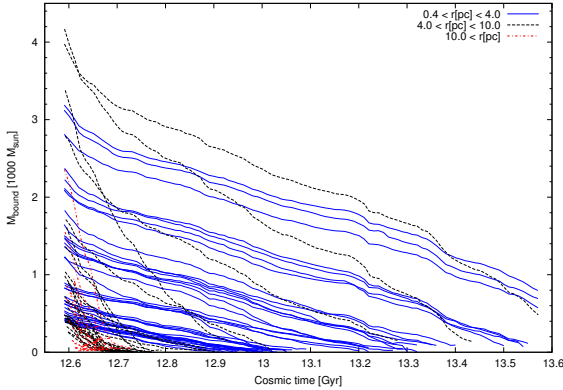


**Figure 6.8:** Mass evolution of clusters in tidal field 30.

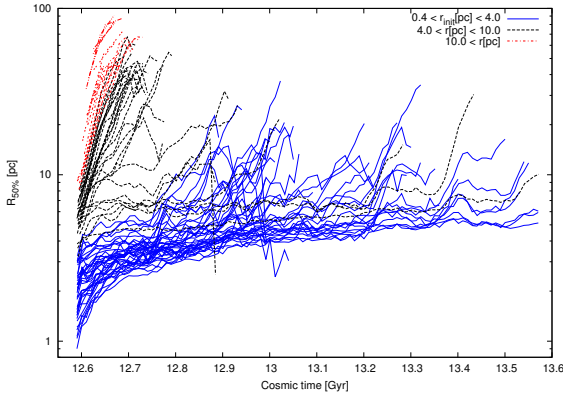


**Figure 6.9:** Half-mass radius evolution of clusters in tidal field 30.

Since the more extended clusters are quickly destroyed, the radius distribution of the clusters soon converges to smaller radii. In fact, as early as 200 Myr after the clusters are born, we see a half-mass radius distribution that has a peak between 4–5 pc, regardless of the tidal field. Clusters with an initially more compact radius gradually move towards this radius, while clusters with a half-mass radius larger than 7 pc are destroyed within 100 Myr (as seen in Figures 6.8 and 6.9 for tidal field 30, as an example).

### 6.3.3 Comparison to observed open clusters

In Figure 6.10, we plot the mass vs age distribution of surviving clusters, normalized to the number of clusters in the initial distribution. Each age bin represents an individual tidal field, each of which contains 100 clusters initially. In the same figure, we overplot the masses and ages of observed clusters, using the open cluster catalog data from Lamers et al. (2005); Kharchenko et al. (2005). The masses of

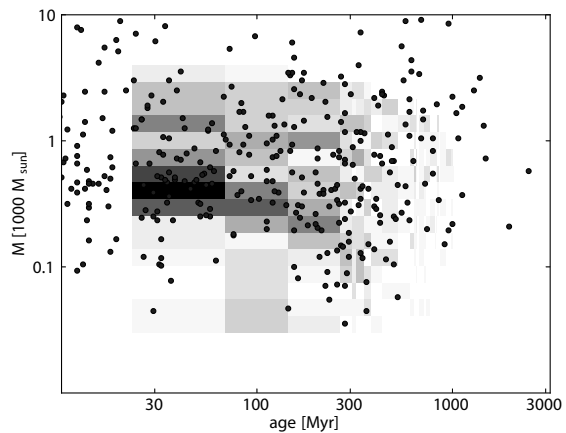


**Figure 6.10:** Distribution of simulated clusters surviving until  $z = 0$  (background, greyscale) with observed clusters from Lamers et al. (2005); Kharchenko et al. (2005) overlotted.

these observed clusters were obtained by fitting a Salpeter mass function with a lower limit of  $0.15 M_{\odot}$  to all observed stars.

Both the simulated and the observed distribution show a lack of clusters older than  $\approx 1$  Gyr, which was earlier identified as the "Oort problem". Also, both distributions show a peak in mass around  $500 M_{\odot}$  at young age, which declines with age.

The initial population of simulated clusters has a cutoff on the high end of the mass distribution at  $> 5000 M_{\odot}$ , as a result the simulated cluster distribution shows a dearth of higher-mass clusters especially at later ages.

#### 6.3.4 Influence of eccentricity on cluster properties

In Table 6.2 we show the masses, ages and radii for surviving clusters, divided into four categories based on their final mass and the eccentricity of their orbit in the galaxy. We find that clusters on orbits with high eccentricity show a larger half-mass radius than those clusters on more circular orbits. This may be a result of the more strongly varying tidal field experienced by these clusters. The low-mass clusters also show a larger half-mass radius than the high-mass sample. This is likely a result of nearly-disrupted clusters being included in this sample.

For clusters with equal mass, we find a higher age in the low-eccentricity cases than in high-eccentricity cases. This is a result of the stronger tidal field, and therefore mass loss, experienced by the latter group.

#### 6.3.5 White dwarfs as a signature for tidal field strength

In the initial phase of our star clusters, masses selected from a Kroupa (2001) mass function are assigned randomly to stars. In evolved clusters however, mass segrega-

**Table 6.2:** Properties of surviving simulated clusters, for clusters with high ( $> 0.129$ ) and low eccentricity, and high ( $> 458 M_{\odot}$ ) and low mass.

	N	$\langle M \rangle$ $M_{\odot}$	$\sigma M$ $M_{\odot}$	$\langle \text{age} \rangle$ Myr	$\sigma \text{ age}$ Myr	$r$ pc	$\sigma r$ pc
Low e, low mass	139	190	130	380	170	7.7	5.2
Low e, high mass	126	1190	590	430	210	4.9	1.9
High e, low mass	133	200	130	270	270	15.5	17.2
High e, high mass	147	1150	670	360	330	5.9	8.9

**Table 6.3:** Properties of two clusters of similar mass and radius at  $z = 0$ .

Cluster	Tidal field	$M_{\text{bound}}$ $M_{\odot}$	$R_{50\%}$ pc	$N_{\text{WD}}$
C004	T14	1253	4.8	54
C027	T15	1227	4.3	29

tion has been observed (e.g. Brandl et al. 1996; de Grijs et al. 2002), where massive stars have preferentially migrated towards the core. Since a tidal field preferentially removes stars from the outer parts of the cluster, over time tidal disruption in combination with mass segregation will increase the average stellar mass in the cluster.

In the case where the tidal field is initially weak, mass segregation can take place before a significant number of stars is stripped from the cluster, allowing these stars to be preferentially low-mass. In a strong tidal field however, mass stripping will occur before mass segregation. In such a cluster, higher-mass stars would be stripped as well, leading to a different fraction of high-mass stars in the cluster.

At a later age, this difference may translate into a different fraction of stellar remnants such as white dwarfs in the cluster. In order to test this scenario, we select two clusters from two tidal fields that differ in strength, but little in age (tidal fields 14 and 15, see Table 6.1), to investigate in more detail. These clusters originate from different masses, yet show similar characteristics ( $M_{\text{bound}}$ ,  $R_{50\%}$ , see Table 6.3) at  $z = 0$ . However, the number of white dwarfs within  $R_{50\%}$  is much higher in cluster 004. In order to test our hypothesis that this difference is a signature of the different strength of the tidal field, we re-simulate both these clusters for 130 different realizations of the initial random seed, and compare the characteristics.

In Table 6.4, we show the results of these new realizations. We count the number of white dwarf stars within  $R_{50\%}$  for each of these realisations, and show the average and standard deviation of this number. We find that the cluster that experienced the weaker tidal field, C027, now contains a slightly larger number of

**Figure 6.11:** Mass evolution of the 130 times re-simulated clusters T14 C004 and T15 C027. Solid lines represent the averaged value, dashed lines represent the  $1\sigma$  variation.

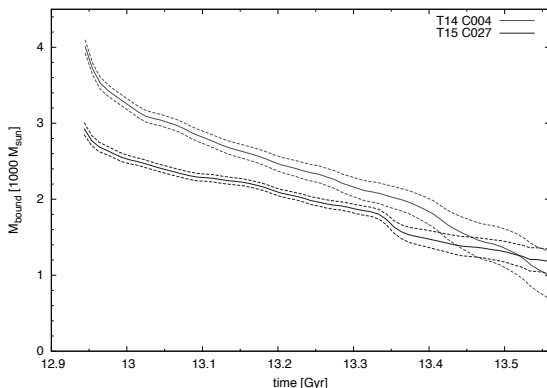


**Table 6.4:** Properties of 130 re-simulated clusters.

Cluster	Tidal field	$N_{\text{surv}}$	$M_{\text{bound}}$ $M_{\odot}$	$R_{50\%}$ pc	$N_{\text{WD}}$	$N_{\text{WD}}/M_{\text{bound}}$ $1/M_{\odot}$
C004	T14	128	$930 \pm 310$	$4.7 \pm 0.5$	$34.2 \pm 14.4$	0.037
C027	T15	130	$1130 \pm 170$	$4.4 \pm 0.5$	$42.6 \pm 9.6$	0.038

white dwarf stars at  $z = 0$ . However, when we count the number of white dwarfs per mass unit, this difference disappears. Based on these simulations, we find no evidence of the tidal field strength based on the number of white dwarfs.

## 6.4 Discussion and conclusions

We used a self-consistent model to simulate star clusters in a Milky Way-type galaxy. The clusters simulated in this way are disrupted in the first 1.1 Gyr, a result that is in agreement with observations and earlier studies.

## Acknowledgements

*We are grateful to Arjen van Elteren, Inti Pelupessy and Nathan de Vries, for their assistance with and work on AMUSE. Likewise, we are grateful to Jeroen Bédorf for his work on Bonsai. Furthermore, we would like to express our gratitude to Henny Lamers for useful discussions and assistance with observed cluster data, and to Nate Bastian and Mark Gieles for useful and interesting discussions*